Rozen's Epoxidation Reagent, $CH_3CN{\cdot}HOF$: A Theoretical Study of Its Structure, Vibrational Spectroscopy, and Reaction Mechanism†

Rotem Sertchook

Departments of Organic Chemistry and Structural Biology, Weizmann Institute of Science, IL-76100 Rehovot, Israel

A. Daniel Boese

Institute of Nanotechnology, Forschungszentrum Karlsruhe, P.O. Box 3640, D-76021 Karlsruhe, Germany

Jan M. L. Martin*

Department of Organic Chemistry, Weizmann Institute of Science, IL-76100 Rechovot, Israel

Received: September 27, 2005; In Final Form: October 31, 2005

Rozen's epoxidation reagent, $CH_3CN{\cdot}HOF$, and a prototype epoxidation reaction employing it, have been subjected to an extensive ab initio and density functional study. Its anharmonic force field reveals a very strong red shift for the OH stretch and a strong blue shift for the HOF bend, in semiquantitative agreement with experiment. The very strong hydrogen bond (8.20 kcal/mol at the W1 level) not only serves to stabilize the reactant but also considerably lowers the barrier height for epoxidation of ethylene. Moreover, the reaction byproduct HF is found to act autocatalytically. The OH moiety acquires HO^+ character in the transition state. Our W1 benchmark data for the reaction profile allow the performance of various DFT functionals to be assessed. In general, "kinetics" functionals overestimate barrier heights, the BMK functional less so than the others. The B1B95 and TPSS33B95 meta-GGA functionals both perform very well, whereas general-purpose hybrid GGAs underestimate barrier heights. The simple PBE0 functional does reasonably well.

I. Introduction

Hypofluorous acid (HOF) was first synthesized by Studier and Appelman[1] in 1971. It was, however, found to be a very unstable substance—at room temperature, decomposition of gaseous HOF to HF and $^1/_2O_2$ has a half-life of about 1 h, and the liquid has a tendency to explode at temperatures above −40 °C (in the presence of oxidizable material even at −78 °C).[2]

In 1986, Rozen and co-workers[3] found a way both to stabilize the compound and to harness it as a synthetic reagent by complexation with acetonitrile. By bubbling an N_2 stream containing about 10% F_2 through an aqueous acetonitrile solution (10% H_2O), a $CH_3CN{\cdot}HOF$ complex is created that has a half-life of several hours at room temperature.

The great synthetic value of HOF results from its unique structure in which an oxygen atom is bonded to the only more electronegative element, fluorine, thus turning the oxygen into a strong electrophile. As such, HOF and $CH_3CN{\cdot}HOF$ are extremely powerful oxygenating and hydroxylating agents.

$CH_3CN{\cdot}HOF$ can be used under very mild reaction conditions and can perform oxidative transformations of which other reagents are incapable. It will epoxidize any double bond, including very deactivated ones, rapidly and with high yields.[4−7] It also efficiently oxidizes amines to nitro derivatives[8−11] and transforms sulfides, even highly deactivated ones, into the corresponding sulfones.[12,13] It is also useful for hydroxylation α to a carbonyl of many ketones, esters, and acids[14,15] and many related transformations.[16,17] Reactions are usually complete in a few minutes at temperatures ranging from 0 to 25 °C.

A number of mechanistic questions arise here, not only as to the mechanism of the reaction but also as to the role of CH_3CN: is it merely an otherwise inert reactant stabilizer, does it have a passive solvent role, or does it actively assist the reaction?

In an attempt to answer these questions, we carried out a computational study on the mechanism of a prototype reaction, namely epoxidation of the simplest olefin by $CH_3CN{\cdot}HOF$:

$$H_2C{=}CH_2 + HOF \xrightarrow{[CH_3CN]} H_2C\overset{O}{\frown}CH_2 + HF \qquad (1)$$

To the best of our knowledge, this system has not previously been subjected to any theoretical studies, and available experimental data are very limited. In the present work, we will apply modern density functional theory (DFT) methods to the mechanism of this reaction and validate our DFT findings by means of high-accuracy ab initio calculations on the smaller systems. We will also consider the formation of alternative hydrogen bond networks (via the reaction products HF and/or F^-). Finally, we will obtain DFT anharmonic force fields of the $CH_3CN{\cdot}HOF$ dimer and its monomers, in an effort to assist future spectroscopic studies on the dimer.

II. Computational Details

All DFT calculations were carried out using a locally modified version of Gaussian 03 Revision C.01.[18] Initially, we employed the B97-1 hybrid GGA (generalized gradient approximation)

† Part of the "Chava Lifshitz Memorial Issue".

* Corresponding author. E-mail: comartin@wicc.weizmann.ac.il.

10.1021/jp055487i CCC: $33.50
Published on Web 12/06/2005

functional, which represents the Handy group reparametrization[19] of Becke's 1997 hybrid GGA.[20] (This functional has 21% Hartree−Fock type "exact" exchange.) B97-1 was previously shown to yield excellent performance for equilibrium properties in general,[19,21] and for hydrogen bonds in particular.[22]

To give a realistic representation of the energetics and kinetics of the reaction, the DFT functional chosen should correctly reproduce both the reaction barriers and the hydrogen bond energies. As this combination is a rather difficult task for present-day DFT methods, we have considered a rather wide variety of functionals and validated them against benchmark ab initio calculations (see below). Our specific choices were to some extent motivated by our recent findings[23] in a validation study on a number of late transition metal catalyzed reactions. Besides the B3LYP[24,25] and PBE0[26] hybrid GGA functionals, we considered the following hybrid meta-GGA functionals:

- BMK (Boese−Martin for kinetics[21])
- TPSS1KCIS, i.e., Tao−Perdew−Staroverov−Scuseria meta-GGA exchange[27] with Krieger−Chen−Iafrate−Savin meta-GGA correlation[28] and 13% HF exchange, a combination proposed by Truhlar and co-workers[29]
- Becke's B1B95 functional,[30] which combines Becke's meta-GGA correlation functional[30] with Becke's GGA exchange[31] and 28% exact exchange
- BB1K, Truhlar's kinetics variant[32] (with 42% exact exchange) of the previous functional
- the mPW1B95 and mPWB1K functionals,[33] which combine modified Perdew-Wang exchange[34−36] with B95 correlation, and 31 and 44% exact exchange, respectively
- Truhlar's very recent PW6B95 and PWB6K functionals[37]
- the TPSS25B95 and TPSS33B95 functionals proposed by Quintal et al.,[23] which are combinations of TPSS exchange with B95 correlation using 25 and 33% HF exchange, respectively
- the very recent M05 (Minnesota-2005) functional of Truhlar and co-workers.[38]

Jensen's polarization consistent[39−42] basis sets were used for all DFT calculations. Initial optimizations were carried out using the fairly small aug-pc1 basis set (which is of 3s2p1d+diffuse spd quality on first-row atoms). Further refinements employed the much more extensive aug-pc2 basis set, which is of 4s3p2d1f+diffuse spdf quality. This large basis set was used not only to minimize basis set truncation error on the computed properties but also to reduce BSSE (basis set superposition error) on the H-bonded energies as far as possible. Finally, to check the basis set convergence, some single-point calculations were carried out using the aug-pc3 basis set, which is of 6s5p4d2f1g+diffuse spdfg quality.

Unless noted otherwise, geometries for the various species involved in this reaction were fully optimized at the respective levels of theory, and vibrational frequencies calculated to both characterize the stationary point and obtain zero-point vibrational energies (ZPVEs) and (rigid rotor-harmonic oscillator) thermal corrections. Subsequently, intrinsic reaction coordinate[43,44] (IRC) calculations were carried out on the transition states to verify that the computed transition states were indeed saddle points between reactants and products. Solvation effects were approximated using a static isodensity surface polarized continuum model (IPCM)[45] with acetonitrile as the solvent ($\epsilon = 36.64$).

To validate the DFT calculations, selected reaction and association energies were also obtained by means of the W1 (Weizmann-1) ab initio computational thermochemistry protocol.[46−48] Basically, W1 theory represents an extrapolation to the relativistic, infinite basis set, CCSD(T) limit: as documented elsewhere,[46−48] errors in total atomization energies (TAEs) are typically in the kJ/mol range, and should therefore definitely be accurate enough for our purpose. We note that W1 theory has recently been used by several groups[21,49,50] for generating benchmark data for parametrizing and validating DFT methods. The actual calculations were carried out by means of the MOLPRO 2002 electronic structure package[51] and a driver script written in Perl.[52]

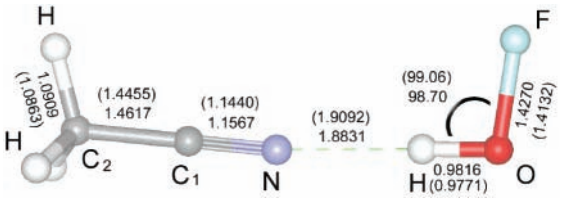

Figure 1. B97-1/aug-pc2 and (in parentheses) B1B95/aug-pc2 optimized structures (Å, degrees) for $CH_3CN{\cdot}HOF$

To facilitate future experimental spectroscopic studies on the $CH_3CN{\cdot}HOF$ complex, we carried out an anharmonic force field study on this system. Following the approach first proposed by Schneider and Thiel,[53] a full cubic and a semidiagonal quartic force field are obtained by central numerical differentiation (in rectilinear normal coordinates about the equilibrium geometry) of analytical second derivatives. The latter were obtained by means of locally modified versions of Gaussian 03;[18] modified routines from CADPAC[54] were used as the driver for the numerical differentiation routine. All the force fields have been analyzed by means of the SPECTRO[55] and POLYAD[56] rovibrational perturbation theory programs developed by the Handy and Martin groups, respectively. In all cases, when strong Fermi resonances lead to band origins perturbed more than about 2 cm^{-1} from their second-order position, the deperturbed values are reported and resonance matrices diagonalized to obtain the true band origins. As second-order rovibrational perturbation theory leads to unphysical anharmonicities involving the very low-lying intermonomer vibrations in the complex, we have deleted all anharmonicity constants involving these three modes from the analysis.

III. Results and Discussion

A. Structure and Energetics of the $CH_3CN{\cdot}HOF$ Complex. At the B97-1/aug-pc2 level of theory, we find the $CH_3CN{\cdot}HOF$ complex to have C_s symmetry. Its optimized structure is presented in Figure 1. The computed and experimentally derived equilibrium structural parameters of the complex and its constituent monomers are presented in Table 1, together with available experimental data. The latter include a spectroscopic r_e geometry for the HOF molecule,[57] an old r_z[58] and a more recent approximate r_e structure[59] for the acetonitrile molecule,[58] and fairly crude X-ray diffraction data for the complex[2]. (For a concise overview of the different geometry types, see Kuchitsu.[60])

In general, agreement between the computed monomer geometries and the available r_e data is very satisfactory, with computed values lying within or near experimental standard deviation bands. Larger deviations are found for the OF bond length, which is underestimated by 0.012 Å, and for the HOF angle, which is overestimated by 1.2°, although we note that the standard deviation on the experimental measurement is itself 0.5°. (It has been shown repeatedly (e.g., refs 61−63) that correlation effects in the OF bond represent a particular challenge for electronic structure methods in general and density functional theory in particular.) The large reported uncertainties in the crystallographic study of the $CH_3CN{\cdot}HOF$ complex[2] render any comparison with the computed data somewhat futile.

TABLE 1: B97-1/aug-pc2 and Experimental Geometric Parameters for HOF, CH_3CN, and $CH_3CN{\cdot}HOF$[a]

	monomers	exp	complex	exp[e]
		Bond Lengths (Å)		
r(F−O)	1.4223	1.4350(31)[b]	1.4270	1.30(1)
r(O−H)	0.9689	0.9657(16)[b]	0.9816	1.1(1)
r(H ⋯N)			1.8831	1.7(1)
r(N−C_1)	1.1520	1.1567(6),[c] 1.156(2)[d]	1.1495	1.15(1)
r(C_1−C_2)	1.4578	1.4617(2),[c] 1.457(2)[d]	1.4555	1.45(1)
r(C_2−H)	1.0909	1.0947(24),[c] 1.087(3)[d]	1.0910	
		Angles (deg)		
∠FOH	98.71	97.54(50)[b]	98.70	93(5)
∠OHN			179.4	177(9)
∠CCN	110.05	109.1(1),[c] 110.1(3)[d]	109.87,[f] 109.80[g]	

[a] Experimental uncertainties shown in parentheses represent $\pm 1\sigma$ in the least significant digits. See Figure 1 for numbering of atoms. [b] r_e geometry, ref 57. [c] r_z geometry, ref 58. [d] Approximate r_e geometry, ref 59. [e] X-ray diffraction, ref 2. [f] Out of symmetry plane. [g] In symmetry plane.

TABLE 2: APT Charges for Free and Complexed HOF and CH_3CN Molecules Obtained from B97-1/aug-pc2 Calculations

	monomers	complex	D
F	−0.2126	−0.2502	−0.0376
O	−0.0572	−0.1876	−0.1304
H	0.2698	0.4703	0.2005
N	−0.3218	−0.4128	−0.091
C_1	0.1149	0.1763	0.0614
C_2	0.0904	0.0553	0.4626
3 × H	0.0388	0.0496	0.0108

On the basis of the level of agreement with experiment for the monomeric geometries, however, we have reason to believe that our computed geometry for the complex is reliable and provides a solid basis for further analysis.

As can be seen from Table 1, the geometries of the monomer units in the complex do not differ significantly from the free monomer structures. As expected, however, a certain amount of charge rearrangement is observed in the APT (atomic polar tensor[64]) charges (Table 2): the APT positive partial charge on the hydrogen-bonded atom, and the negative partial charges on the adjacent oxygen and nitrogen atoms become considerably more pronounced. The APT charges in free HOF (+0.212 e on the OH moiety) are in qualitative agreement with earlier rough estimates (+0.5 e on the OH moiety) derived from NMR chemical shifts in liquid HOF.[65]

To illustrate the reliability of W1 as a primary standard for thermochemical calculations, we will consider the heats of formation of some of the species involved in the reaction under study (and in the H-bonded complexes). In a previous validation study,[48] we found that W1 theory reproduces the well-established heats of formation of CH_3CN, C_2H_4, HF, and C_2H_4O to within +0.3, +0.6, +0.4, and −0.2 kcal/mol, respectively. For hypofluoric acid, we calculate $\Delta H°_{f,0} = -19.89$ and $\Delta H°_{f,298} = -20.60$ kcal/mol, the former in excellent agreement with the recently revised value of Peterson and co-workers,[66] $\Delta H°_{f,0} = -20.02 \pm 0.25$ kcal/mol.

At the B97-1/aug-pc2 level, the dissociation energy of the $CH_3CN{\cdot}HOF$ complex (Table 3) is found to be 8.26 kcal/mol in the gas phase and 5.08 kcal/mol in a simulated CH_3CN solvent. The gas-phase value is in excellent agreement with the W1 value, 8.20 kcal/mol. This strong hydrogen bond energy certainly explains the stabilization of HOF within the complex. From the B97-1/aug-pc2 computed enthalpy of dissociation at 298 K, 6.81 kcal/mol, and assuming the solvent effect to be transferable from the bottom of the well, we find an estimated enthalpy of dissociation at 298 K of 3.63 kcal/mol. Assuming the difference between B97-1/aug-pc2 and W1 theory to be likewise transferable, our final best estimate is 3.57 kcal/mol. Agreement with the experimental value of Appelman et al.,[67] 3.42 ± 0.12 kcal/mol, is as good as we can reasonably expect.

TABLE 3: Computed DFT and W1 Dissociation Energies (kcal/mol) of Hydrogen Bonds in $CH_3CN{\cdot}HOF$, $CH_3CN{\cdot}HF$, and $C_2H_4O{\cdot}HF$

	$CH_3CN{\cdot}HOF$		$CH_3CN{\cdot}HF$		$C_2H_4O{\cdot}HF$	
	vacuum	CH_3CN	vacuum	CH_3CN	vacuum	CH_3CN
B97-1/aug-pc1	9.55		10.13		10.83	
B97-1/aug-pc2	8.26	5.07	9.43	6.50	9.56	7.06
B97-1/aug-pc3[a]	8.10		9.29		9.40	
BMK/aug-pc2[a]	7.49		8.85		9.17	
B3LYP/aug-pc2	7.99		9.27		9.38	
PBE0/aug-pc2	8.35	5.46	9.65	6.99	9.62	7.12
B1B95/aug-pc2	7.06	2.38	8.28	4.99	8.05	5.62
TPSS33B95/aug-pc2[b]	8.11	3.33	9.28	5.74	9.31	6.72
M05/aug-pc2[b]	8.28		9.50		9.08	
mPWB1K/aug-pc2[b]	7.88	2.90	9.03	5.30	8.94	6.22
W1 theory	8.20		9.06		9.80	

[a] At B97-1/aug-pc2 geometry. [b] At B1B95/aug-pc2 geometry.

Even stronger hydrogen bonds are seen in the $CH_3CN{\cdot}HF$ and $C_2H_4O{\cdot}HF$ complexes (9.06 and 9.80 kcal/mol, respectively, at the W1 level). B97-1/aug-pc2 reproduces all of these rather well; single-point B97-1/aug-pc3 calculations at the B97-1/aug-pc2 geometry lower all the binding energies by 0.14−0.16 kcal/mol compared to aug-pc2, suggesting that the aug-pc2 basis set is sufficiently close to the basis set limit. (The aug-pc1 basis set is definitely inadequate.) Of the other functionals considered, PBE0, B3LYP, and TPSS33B95 all perform about as well as B97-1, whereas mPWB1K and BMK are somewhat inferior and B1B95 clearly underestimates the hydrogen bond energies.

B. Vibrational Frequencies. Vibrational frequencies beyond the harmonic approximation were obtained by means of second-order rotation−vibration perturbation theory from a semidiagonal quartic force field obtained at the B97-1/aug-pc1 level and harmonic frequencies obtained at the B97-1/aug-pc2 level. This level of theory was shown previously[68−70] to yield sufficiently reliable anharmonic vibrational frequencies for most purposes: sadly, large basis set CCSD(T) harmonic frequencies are not a practical option for the complex. As for the monomers, Breidung et al.[71] and Peterson and co-workers[66] previously obtained accurate CCSD(T) anharmonic force fields for HOF, whereas in a very recent study by Pouchan and co-workers[72] on CH_3CN, a B3LYP/cc-pVTZ anharmonic force field was combined with CCSD(T)/cc-pVTZ harmonic frequencies.

Calculated harmonic and fundamental frequencies of the free monomers and the $CH_3CN{\cdot}HOF$ complex are presented in Table 4, together with the available experimental and selected ab initio data. For the monomers, harmonic frequencies are generally in good agreement with experiment or accurate ab initio values, except for the OF stretch in HOF and (to a lesser extent) the CN and CC stretching frequencies in CH_3CN. (The aforementioned difficulties of DFT with describing OF bonds are seen here in amplified form.) As for the CN and CC stretches in CH_3CN, one of the main consequences of the errors in these harmonic frequencies is that the observed $\nu_3 + \nu_4 \approx \nu_2$ Fermi type 2 resonance is nearly absent in this computed spectrum.

As in the majority of hydrogen-bonded systems, the vibrational modes of the isolated monomers remain largely recognizable in the complex. A comparison of the vibrational modes of the complex to the corresponding modes of the isolated monomers (Table 4) reveals that spectral perturbations in the

TABLE 4: Harmonic and Fundamental Vibrational Frequencies (cm^{-1}) for Free and Complexed HOF and CH_3CN Molecules

B97-1/aug-pc1		B97-1/aug-pc2		ab initio[b,e]		experiment		
ω	ν	ω	ν	ω	ν	ω	ν	assignment
				HOF				
3734.5	3546.5	3765.3	3582.5	3780.9[b]	3591.0[b]	3763.95 ± 4.6[c]	3577.9[d]	OH stretch
1408.4	1367.2	1420.0	1380.0	1405.1[b]	1361.1[b]	1396.22 ± 7.0[c]	1353.4[d]	HOF bend
971.0	951.0	1002.7	982.1	921.4[b]	893.8[b]	916.84 ± 19[c]	889.1[d]	OF stretch
				CH_3CN				
3047.4	2934.0	3044.4	2936.8	3065[e]	2970[e]	3044[f]	2954.1[g]	CH_3 stretch (A_1)
2359.7	2328.8	2355.5	2327.2	2297[e]	2247[e]	2294[f]	2266.5[g]	CN stretch (A_1)
1391.7	1358.4	1404.4	1369.4	1413[e]	1376[e]	1418[f]	1385.0[g]	CH_3 deform. (A_1)
932.9	926.0	1002.7	919.9	920[e]	913[e]	929[f]	920.2[g]	CC stretch (A_1)
3133.2	2989.2	3121.0	2979.3	3149[e]	3053[e]	3135	3009.2[g]	CH_3 stretch (E)
1459.3	1429.6	1470.1	1438.7	1487[e]	1486[e]	1478[f]	1447.9[g]	CH_3 deform. (E)
1049.7	1037.0	1056.3	1034.8	1061[e]	1038[e]	1062[f]	1040.8[g]	CH_3 rock (E)
371.7	374.8	377.9	380.9	361[e]	364[e]	365[f]	362[g]	CCN bend (E)

gas phase				pcm(argon)				
B97-1/aug-pc1		B97-1/aug-pc2		B97-1/aug-pc1		experiment		
ω	ν	ω	ν	ω	ν	ω	ν	assignment
				$CH_3CN{\cdot}HOF$				
3502.8	3298.1[h]	3521.9	3316.6[i]	3450	3251[j]		3230[k]	OH stretch
1506.1	1453.2	1516.6	1457.4	1510	1458		1437[k]	HOF bend
964.4	942.9	994.6	975.3	963	942		881[k]	OF stretch
3049.6	2935.4	3047.3	2936.3	3047	2932			CH_3 stretch
2384.0	2349.2	2376.2	2342.6	2382	2347			CN stretch
1391.3	1358.4	1403.4	1370.5	1389	1356			CH_3 deform.
941.7	933.2	934.2	926.1	941	933			CC stretch
3138.6	2988.2	3126.5	2974.2	3137	2987			CH_3 QD stretch
1455.7	1425.4	1466.0	1435.3	1452	1425			CH_3 QD deform.
1050.2	1027.1	1055.6	1032.1	1049	1026			CH_3 QD rock
378.2	376.3	383.1	384.7	382	381			CCN QD bend
610.5	556.0	606.5	554.8	629	572			OH o-o-p wrt CN

[a] QD=quasidegenerate. Experimental uncertainties are ± 1σ. [b] Large basis set CCSD(T)+core-valence+scalar relativistic corrections, ref 66. [c] Reference 57. [d] Reference 78. [e] CCSD(T)/cc-pVTZ, ref 72. [f] Reference 79. [g] Reference 80. [h] In Fermi resonance with HOF bend overtone at 2861.2 cm^{-1}: deperturbed band origins at 3254.6 and 2904.8 cm^{-1}, respectively, and $W = 261.7$ cm^{-1}. [i] In Fermi resonance with HOF bend overtone at 2861.4 cm^{-1}: deperturbed band origins at 3276.1 and 2901.9 cm^{-1}, respectively, and $W = 259.2$ cm^{-1}. [j] In Fermi resonance with HOF bend overtone at 2866 cm^{-1}: deperturbed band origins at 3203 and 2915 cm^{-1}, respectively, and $W = 255.1$ cm^{-1}. [k] In argon/helium matrix, ref 67.

CH_3CN moiety are rather small (less than 20 cm^{-1}), whereas much stronger shifts are seen in the FOH moiety. Specifically, the O−H stretching vibration is red-shifted by 248 cm^{-1}, and the FOH bending mode exhibits a blue shift of 86 cm^{-1}. The blue shift for the FOH bending mode is in very good agreement with that found experimentally by Appelman et al.,[67] but these authors report an extremely large red shift of almost 350 cm^{-1} on the OH stretch that is only in semiquantitative agreement with our calculations. The OH red shift in the complex causes sufficient narrowing of the gap with the HOF bend overtone that significant Fermi type 1 resonance occurs. (As can be seen in the footnotes to Table 4, the cubic anharmonicity constant linking these two vibrations is very large.)

For HOF, comparison between experimental gas-phase and noble gas matrix IR spectra from different sources[75,73] leads to conflicting conclusions: although matrix red shifts of only 1−6 cm^{-1} were found by Appelman et al.,[75] one of the researchers involved in refs 2 and 67 reports a red shift of 25 cm^{-1} for the OH mode in Table 15 of his Ph.D. thesis.[73] (Appelman et al.[75] found a matrix red shift of 41 cm^{-1} in N_2.) Comparison between B97-1/aug-pc2 harmonic frequency calculations on HOF in the gas phase and using a PCM model[74] with argon as the "solvent" reveals a large computed red shift of 67 cm^{-1}: literature evidence[76] suggests that medium shifts calculated using the PCM model are semiquantitative at best, yet the calculation would seem to indicate a significant red shift.

We therefore carried out an anharmonic force field calculation for the entire complex at the PCM-B97-1/aug-pc1 level. The results (Table 4) suggest a red shift of about 53 cm^{-1} on the unperturbed HO stretch; narrowing of the Fermi resonance gap, and the resulting increased perturbation, reduce the matrix shift to about 47 cm^{-1}. Our computed HOF stretching frequency in Ar matrix, 3251 cm^{-1}, is actually in rather good agreement (perhaps to some extent fortuitously) with the experimental observation at 3230 cm^{-1}.

Appelman et al. also report a strong and broad band at 2860 cm^{-1}, which shifts to 2113 cm^{-1} upon deuteration. On the basis of our calculations, we assign these bands to the overtone of the HOF viz. DOF bend (calculated at 2904 and 2134 cm^{-1}, respectively, in the gas phase at the B97-1/aug-pc2 level, and at 2866 and 2140 cm^{-1}, respectively, in PCM argon at the B97-1/aug-pc1 level).

Dunkelberg[73] reports an even larger red shift, to 3141 cm^{-1}, in CH_3CN at −150 °C: at the PCM-B97-1/aug-pc1 level, we find a deperturbed fundamental at 2953 cm^{-1} (very close to the HOF overtone at 2916 cm^{-1}) and a perturbed fundamental at 3053 cm^{-1}. Once again, PCM reproduces this medium effect qualitatively but not quantitatively.

C. Mechanism and Kinetics for the Epoxidation Reaction. At the B97-1/aug-pc2 level and in the gas phase, the epoxidation of ethylene by free HOF is calculated to be exothermic by $\Delta E_e = -68.6$ kcal/mol and exergonic by $\Delta G_{298} = -65.8$ kcal/mol. The former value is in very good agreement with our W1 result, $\Delta E_e = -71.00$ kcal/mol. With $CH_3CN{\cdot}HOF$ as the reactant, the reaction is likewise highly exothermic (ΔE_e −69.8 kcal/mol, ΔG_{298} −66.0 kcal/mol).

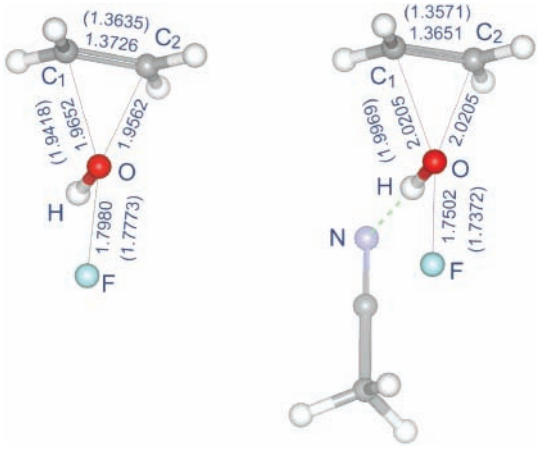

Figure 2. B97-1/aug-pc2 and (in parentheses) B1B95/aug-pc2 optimized structures (Å, degrees) for the epoxidation transition state, with (a) HOF and (b) $CH_3CN{\cdot}HOF$ as reactants.

The epoxidation transition state structure in both cases, bare HOF and $CH_3CN{\cdot}HOF$, is displayed in Figure 2. In both cases, r(O−F) is stretched by over 0.3 Å compared to the reactant, but r(C═C) is elongated by only 0.04 Å, and r(C···O) of about 2 Å likewise indicates no epoxide bonds have been formed yet. This relatively "early" transition state is consistent with the Hammond postulate and the very exothermic character of the reaction. According to the APT charge distribution, the HOF moiety acquires HO^+ F^- character in the transition state, with partial charges of +0.86 and −0.86 *e*, respectively, without CH_3CN and +0.90 and −0.94 *e*, respectively, with hydrogen-bonded CH_3CN.

The strongly polar character of the transition state also expresses itself in the rather slow basis set convergence for the barrier height: it still increases by 0.44 kcal/mol between aug-pc2 and aug-pc3 basis sets, compared to −0.10 kcal/mol for the overall reaction energy. (The aug-pc1 basis set is clearly woefully inadequate.)

Reproduction of reaction barrier heights continues to be an Achilles heel of density functional theory,[21,77] and indeed the B97-1/aug-pc2 barrier is too low, relative to the W1 value, by 4.45 kcal/mol, of which only 10% can be attributed to basis set incompleteness. Various "kinetics" functionals such as PWB6K, BB1K, and mPWB1K seriously (6−10 kcal/mol) overestimate the barrier, the BMK functional less so (3 kcal/mol). The relatively good performance of PW6B95 for the barrier (and the even better one of the very recent M05 functional[38]) are marred by 10 kcal/mol errors in the overall reaction energy. The simple PBE0 functional puts in a fairly creditable performance, and B1B95 reproduces the barrier height almost exactly and TPSS33B95 only slightly overestimates it. TPSS25B95, TPSS1KCIS, and mPW1B95 all underestimate the barrier height.

We were unable to carry out W1 calculations for the reaction with $CH_3CN{\cdot}HOF$, but we can assume that the most reliable results would be obtained from functionals that can handle well both the H-bond energies and the barrier in the absence of CH_3CN. It is thus encouraging that B1B95/aug-pc2 and TPSS33B95/aug-pc2 yield nearly identical results for the barrier heights, even with the limitations of the former in describing the hydrogen bonds. Qualitatively, all functionals show that complexation to CH_3CN lowers the barrier height by 3−4 kcal/mol, and that the already highly exothermic reaction becomes slightly more so, due to the stronger H-bond energy of $C_2H_4O{\cdot}HF$ compared to $CH_3CN{\cdot}HOF$. Consideration of continuum solvent effects further lowers the barriers by 5−7 kcal/mol. (We note that continuum solvent models are *not* a substitute for explicitly considering the hydrogen bond; as can be seen in Table 5, in the absence of an explicit CH_3CN hydrogen bond acceptor, exaggerated solvent effects are found that lead to chemically meaningless negative barrier heights.)

TABLE 5: DFT and W1 Energetics (kcal/mol) for the Epoxidation Reaction

	$\Delta E_e^{\ddagger}$	$\Delta G_{298}^{\ddagger}$	$\Delta E_e^{\ddagger}$(sol)	ΔE_r	ΔE_r(sol)
		HOF			
B97-1/aug-pc1	8.77	18.59	−5.36	−71.29	−75.09
B97-1/aug-pc2	13.81	23.58	−0.09	−68.62	−72.50
B97-1/aug-pc3[a]	14.25			−68.72	
B3LYP/aug-pc2	13.68			−66.22	
BMK/aug-pc2	21.79	31.82		−73.87	
PBE0/aug-pc2	15.47	25.55		−73.07	
TPSS1KCIS/aug-pc2	14.13	24.32		−70.32	
B1B95/aug-pc2	17.66	27.93		−73.76	
BB1K/aug-pc2[b]	24.22			−76.52	
mPW1B95/aug-pc2	15.02	25.23		−73.26	
mPWB1K/aug-pc2[b]	24.24			−77.10	
PW6B95/aug-pc2[b]	21.69			−61.47	
PWB6K/aug-pc2[b]	28.99			−66.15	
TPSS25B95/aug-pc2[b]	15.04			−72.52	
TPSS33B95/aug-pc2[b]	18.89			−74.32	
M05/aug-pc2[b]	16.83			−84.10	
W1	18.26			−71.00	
		$CH_3CN{\cdot}HOF$			
B97-1/aug-pc1	5.82	16.31		−72.22	−84.16
B97-1/aug-pc2	10.66	23.53	5.76	−69.79	−73.93
B97-1/aug-pc3[a]	11.06			−69.91	
PBE0/aug-pc2	12.36	25.48	8.38	−74.37	−78.38
B1B95/aug-pc2	14.71	27.01	8.32	−74.98	−80.22
TPSS33B95/aug-pc2[b]	14.92		8.19	−75.49	−80.69
M05/aug-pc2[b]	13.81			−85.32	
mPWB1K/aug-pc2[b]	19.78		12.70	−78.25	−83.52

[a] Single point calculation at B97-1/aug-pc2 geometry. [b] Single point calculation at B1B95/aug-pc2 geometry.

One potential alternative reaction pathway involves first formation of methyl cyanide *N*-oxide (aka methyl fulminate) $HOF + CH_3CN \rightarrow HF + CH_3CNO$, followed by epoxidation by the fulminate, $CH_3CNO + HC_2{=}CH_2 \rightarrow C_2H_4O + CH_3CN$. Even at the B97-1/aug-pc2 level (where reaction barriers will be underestimated), we found both steps to have unrealistically high barriers, $\Delta G_{298}^{\ddagger} = 41.32$ and 57.19 kcal/mol, respectively.

D. Alternative Hydrogen Bond Assisted Transition State? To investigate possible involvement of other H-bond donors/acceptors in the reaction process, we sought transition states involving F^- and HF, rather than CH_3CN, in the H-bond acceptor role. Optimization at the B97-1/aug-pc2 level led to the structures presented in Figure 3. HF may initially be present in the reaction mixture as a product of the in-situ generation reaction $F_2 + H_2O \rightarrow HOF + HF$ (in the presence of actonitrile) and is of course generated as a byproduct of the epoxidation reaction. Acetonitrile can act as a weak base, and thus some F^- could be present in equilibrium with HF. (However, at the B97-1/aug-pc2 level in a simulated CH_3CN solvent, the reactions $CH_3CN + HF \leftrightarrow CH_3CNH^+F^-$ and $2CH_3CN + HF \leftrightarrow CH_3CN{\cdots}H^+{\cdots}NCCH_3 + F^-$ were both found to be highly endothermic, $\Delta E_e = 38.2$ and 30.2 kcal/mol, respectively. As such, involvement of F^- can safely be ruled out, except in the presence of a strong base, which would also deprotonate HOF.)

The calculated barrier heights (Table 6) show that complexation with HF or F^- significantly lowers the epoxidation reaction barrier, even more so than with CH_3CN itself. (Consistent with the Hammond postulate, the transition state geometries are even

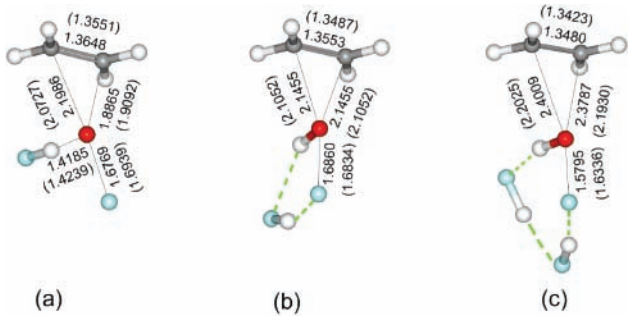

Figure 3. B97-1/aug-pc2 and (in parentheses) B1B95/aug-pc2 optimized structures (Å, degrees) for the epoxidation transition state where the following are hydrogen-bonded to HOF: (a) F^-; (b) a single HF molecule; (c) two HF molecules.

TABLE 6: Epoxidation Reaction Barrier Height with Alternative Hydrogen Bond Donor/Aceptor in the Gas Phase and in CH_3CN Solvent Calculations (in kcal/mol)

	ΔE_e	$\Delta G_{298}^{\ddagger}$	$\Delta E_e^{\ddagger}$(sol)
	F^-		
B97-1/aug-pc2	9.82	20.91	7.27
B1B95/aug-pc2	12.23	23.39	9.26
TPSS33B95/aug-pc2[a]	12.27		8.51
	HF		
B97-1/aug-pc2	3.65	15.63	0.62
B1B95/aug-pc2	7.25	18.98	4.36
TPSS33B95/aug-pc2[a]	7.36		4.24
	2 × HF		
B97-1/aug-pc2	0.09	10.49	−1.08
B1B95/aug-pc2	3.61	14.43	2.12
TPSS33B95/aug-pc2[a]	3.33		1.80

[a] Single point calculation at B1B95/aug-pc2 geometry.

"earlier" than for the CH_3CN complex.) It thus appears that the reaction is accelerated autocatalytically by its own reaction byproducts.

Once again, the B1B95 and TPSS33B95 functionals yield barriers in excellent agreement with each other, whereas B97-1 is systematically too low.

IV. Conclusions

In Rozen's epoxidation reagent, a strong hydrogen bond is formed between HOF and CH_3CN. This hydrogen bond not only stabilizes the reactant but also significantly lowers the epoxidation reaction barrier. The HOF moiety acquires HO^+ F^- character in the transition state. Furthermore, the reaction byproduct, HF, can autocatalytically accelerate the reaction.

Our W1 benchmark data for the reaction profile allow the performance of various DFT functionals to be assessed. In general, "kinetics" functionals exhibit overestimate barrier heights, BMK less so than the others. The B1B95 and TPSS33B95 meta-GGA functionals both perform very well, whereas general-purpose hybrid GGAs underestimate barrier heights. The simple PBE0 functional does reasonably well. In terms of the preferred percentage of Hartree−Fock exchange, this reaction, which has a very polar transition state, seems to take a middle position between main group hydrogen transfer reactions (which prefer elevated HF exchange percentages in the 40−45% range[77,21]) and late transition metal catalyzed reactions (which prefer more typical HF exchange percentages in the 20−25% range[23]).[81]

Acknowledgment. Research was supported by the Israel Science Foundation (grant 709/05), the Minerva Foundation (Munich, Germany), and the Helen and Martin Kimmel Center for Molecular Design. J.M.L.M. is the incumbent of the Baroness Thatcher Professorial Chair of Chemistry and a member ad personam of the Lise Meitner-Minerva Center for Computational Quantum Chemistry. We thank Profs. Shlomo Rozen (Tel-Aviv University, Israel) and David Milstein (Weizmann Institute, Rechovot, Israel) for helpful discussions, and Yan Zhao (Truhlar group, University of Minnesota) for useful information on the M05 implementation.

References and Notes

(1) Studier, M. H.; Appelman, E. H. *J. Am. Chem. Soc.* **1971**, *93*, 2349−2351.
(2) Dunkelberg, O.; Hass, A.; Klapdor, M. F.; Mootz, D.; Poll, W.; Appelman, E. H. *Chem. Ber.* **1994**, *127*, 1871−1875.
(3) Rozen, S.; Brand, M. *Angew. Chem., Int. Ed. Engl* **1986**, *25*, 554−555.
(4) Rozen, S.; Kol, M. *J. Org. Chem.* **1990**, *55*, 5155−5159.
(5) Hung, M. H.; Smart, B. E.; Feiring, A. E.; Rozen, S. *J. Org. Chem.* **1991**, *56*, 3187−3189.
(6) Rozen, S.; Bareket, Y.; Dayan, S. *Tetrahedron Lett.* **1996**, *37*, 531−534.
(7) Dayan, S.; Ben-David, I.; Rozen, S. *J. Org. Chem.* **2000**, *65*, 8816−8818.
(8) Kol, M.; Rozen, S. *J. Chem. Soc., Chem. Commun.* **1991**, 567−568.
(9) Rozen, S.; Kol, M. *J. Org. Chem.* **1992**, *57*, 7342−7344.
(10) Dirk, S. M.; Mickelson, E. T.; Henderson, J. C.; Tour, J. M. *Org. Lett.* **2000**, *2*, 3405−3406.
(11) Golan, E.; Rozen, S. *J. Org. Chem.* **2003**, *68*, 9170−9172.
(12) Rozen, S.; Bareket, Y. *J. Org. Chem.* **1997**, *62*, 1457−1462.
(13) Toyota, A.; Ono, Y.; Chiba, J.; Sugihara, T.; Kaneko, C. *Chem. Pharm. Bull.* **1996**, *44*, 703−708.
(14) Rozen, S.; Bareket, Y.; Kol, M. *Tetrahedron* **1993**, *49*, 8169−8178.
(15) Rozen, S.; Dayan, S.; Bareket, Y. J. *J. Org. Chem.* **1995**, *60*, 8267−8269.
(16) Rozen, S. *Pure Appl. Chem.* **1999**, *71*, 481−487.
(17) Rozen, S. *Acc. Chem. Res.* **1996**, *29*, 243−248.
(18) Frisch, M. J.; et al. *Gaussian 03*, revision C.01;Weizmann local version; 2004.
(19) Hamprecht, F. A.; Cohen, A. J.; Tozer, D. J.; Handy, N. C. *J. Chem. Phys.* **1998**, *109*, 6264−6271.
(20) Becke, A. D. *J. Chem. Phys.* **1997**, *107*, 8554−8560.
(21) Boese, A. D.; Martin, J. M. L. *J. Chem. Phys.* **2004**, *121*, 3405−3416.
(22) Boese, A. D.; Chandra, A.; Martin, J. M. L.; Marx, D. *J. Chem. Phys.* **2003**, *119*, 5965−5980.
(23) Quintal, M. M.; Karton, A.; Iron, M. A.; Boese, A. D.; Martin, J. M. L. *J. Phys. Chem. A* **2006**, *110*, 709−716 (published online October 29, 2005, http://dx.doi.org/10.1021/jp054449w).
(24) Becke, A. D. *J. Chem. Phys.* **1993**, *98*, 5648.
(25) Lee, C.; Yang, W.; Parr, R. G. *Phys. Rev. B* **1988**, *37*, 785.
(26) Adamo, C.; Barone, V. *J. Chem. Phys.* **1999**, *110*, 6158−6170.
(27) Tao, J. M.; Perdew, J. P.; Staroverov, V. N.; Scuseria, G. E. *Phys. Rev. Lett.* **2003**, *91*, 146401.
(28) Krieger, J. B.; Chen, J.; Iafrate, G. J.; Savin, A. In *Electron Correlations and Materials Properties*; Gonis, A., Kioussis, N., Eds.; Plenum: New York, 1999.
(29) Zhao, Y.; Lynch, B. J.; Truhlar, D. G. *Phys. Chem. Chem. Phys.* **2005**, *7*, 43−52.
(30) Becke, A. D. *J. Chem. Phys.* **1996**, *104*, 1040.
(31) Becke, A. D. *Phys. Rev. A* **1988**, *38*, 3098.
(32) Zhao, Y.; Lynch, B. J.; Truhlar, D. G. *J. Phys. Chem. A* **2004**, *108*, 2715−2719.
(33) Zhao, Y.; Truhlar, D. G. *J. Phys. Chem. A* **2004**, *108*, 6908.
(34) Perdew, J. P. In *Electronic Structure of Solids '91*; Ziesche, P., Eschig, H., Eds.; Akademie Verlag: Berlin, 1991.
(35) Burke, K.; Perdew, J. P.; Wang, Y. In *Electronic Density Functional Theory: Recent Progress and New Directions*; Dobson, J. F.; Vignale, G.; Das, M. P., Eds.; Plenum: New York, 1998.
(36) Adamo, C.; Barone, V. *J. Chem. Phys.* **1998**, *108*, 664.
(37) Zhao, Y.; Truhlar, D. G. *J. Phys. Chem. A* **2005**, *109*, 5656−5667.
(38) Zhao, Y.; Schultz, N. E.; Truhlar, D. G. *J. Chem. Phys.* **2005**, *123*, 161103.
(39) Jensen, F. *J. Chem. Phys.* **2001**, *115*, 9113−9125.
(40) Jensen, F. *J. Chem. Phys.* **2002**, *116*, 3502−3502.
(41) Jensen, F. *J. Chem. Phys.* **2002**, *116*, 7372−7379.
(42) Jensen, F. *J. Chem. Phys.* **2002**, *117*, 9234−9240.
(43) Gonzalez, C.; Schlegel, H. B. *J. Chem. Phys.* **1989**, *90*, 2154−2161.

(44) Gonzalez, C.; Schlegel, H. B. *J. Phys. Chem.* **1990**, *94*, 5523−5527.
(45) Foresman, J. B.; Keith, T. A.; Wiberg, K. B.; Snoonian, J.; Frisch, M. J. *J. Phys. Chem.* **1996**, *100*, 16098−16104.
(46) Martin, J. M. L.; de Oliveira, G. *J. Chem. Phys.* **1999**, *111*, 1843−1856.
(47) Martin, J. M. L.; Parthiban, S. In *Quantum Mechanical Prediction of Thermochemical Data*; Cioslowski, J., Ed.; Kluwer Academic: Dordrecht, 2001; Vol. 22, Chapter 2, pp 31−65.
(48) Parthiban, S.; Martin, J. M. L. *J. Chem. Phys.* **2001**, *114*, 6014−6029.
(49) Zhao Y, Gonzalez-Garcia N, T. D. *J. Phys. Chem. A* **2005**, *109*, 2012−2018.
(50) Zhao, Y.; Truhlar, D. G. *J. Chem. Theor. Comput.* **2005**, *1*, 415−432.
(51) Werner, H.-J.; et al. MOLPRO, version2002.6, a package of ab initio programs, 2003; seehttp://www.molpro.net.
(52) Atasoylu, O.; Martin, J. M. L. WN2, an automated driver for the Wn family of computational thermochemistry methods, Weizmann Institute of Science, 2001.
(53) Schneider, W.; Thiel, W. *Chem. Phys. Lett.* **1989**, *157*, 367−373.
(54) Amos, R. D.; et al. The Cambridge Analytic Derivatives Package (Cadpac), Issue 6.5, 1998.
(55) Gaw, J. F.; Willetts, A.; Green, W. H.; Handy, N. C. SPECTRO: a program for the derivation of spectroscopic constants from provided quartic force fields and cubic dipole fields. In *Advances in Molecular Vibration and Collision Dynamics*; Bowman, J. M., Ratner, M. A., Eds.; JAI Press: Greenwich, CT, 1990; Vol. 1B.
(56) Martin, J. M. L. POLYAD: A vibrational perturbation theory program including arbitrary resonance matrices, Weizmann Institute of Science, Rehovot, Israel, 1997.
(57) Halonen, L.; Ha, T. K. *J. Chem. Phys.* **1988**, *89*, 4885−4888.
(58) Demaison, J.; Durbrulle, A.; Boucher, D.; Burie, J.; Typke, V. *J. Mol. Spectrosc.* **1979**, *76*, 1−16.
(59) Le Guennec, M.; Wlodarczak, G.; Burie, J.; Demaison, J. *J. Mol. Spectrosc.* **1992**, *154*, 305−323.
(60) Kuchitsu, K. The Potential Energy Surface and the Meaning of Internuclear Distances. In *Accurate Molecular Structures: their Determination and Importance*; Domenicano, A., Hargittai, I., Eds.; Oxford University Press: Oxford, NY, 1992.
(61) Lee, T. J.; Rice, J. E.; Dateo, C. E. *Mol. Phys.* **1996**, *89*, 1359−1372.
(62) Alcami, M.; Mó, O.; Yánez, M.; Cooper, I. L. *J. Chem. Phys.* **2000**, *112*, 6131−6139.
(63) Kraka, E.; He, Y.; Cremer, D. *J. Phys. Chem. A* **2001**, *105*, 3269−3276.
(64) Cioslowski, J. *J. Am. Chem. Soc.* **1989**, *1111*, 8333−8336.
(65) Hindman, J. C.; Svirmickas, A.; Appelman, E. H. *J. Chem. Phys.* **1972**, *57*, 4542−4543.
(66) Ramachandran, B.; Vegesna, N. S.; Peterson, K. A. *J. Phys. Chem. A* **2003**, *107*, 7938−7944.
(67) Appelman, E. H.; Dunkelberg, O.; Kol, M. *J. Fluorine Chem.* **1991**, *56*, 199−213.
(68) Boese, A. D.; Klopper, W.; Martin, J. M. L. *Mol. Phys.* **2005**, *103*, 863−876.
(69) Boese, A. D.; Klopper, W.; Martin, J. M. L. *Int. J. Quantum Chem.* **2005**, *104*, 830−845.
(70) Boese, A. D.; Martin, J. M. L. *J. Mol. Struct.* **2005**, published online at http//dx.doi.org/10.1016/j.molstruc.2005.07.009.
(71) Breidung, J.; Thiel, W.; Gauss, J.; Stanton, J. F. *J. Chem. Phys.* **1999**, *110*, 3687−3696.
(72) Bégué, D.; Carbonnière, P.; Pouchan, C. *J. Phys. Chem. A* **2005**, *109*, 4611−4616.
(73) Dunkelberg, O. Ph.D. Thesis, Ruhr-Universität Bochum, 1993 (in German).
(74) Cossi, M.; Scalmani, G.; Rega, N.; Barone, V. *J. Chem. Phys.* **2002**, *117*, 43−54 and references therein.
(75) Appelman, E. H.; Downs, A. J.; Gardner, C. J. *J. Phys. Chem.* **1989**, *93*, 598−608.
(76) Cammi, R.; Mennucci, B.; Tomasi, J. Computational modelling of the solvent effects on molecular properties: an overview of the Polarizable Continuum Model (PCM) approach. In *Computational Chemistry: Reviews of Current Trends*; Leszczynski, J., Ed.; World Scientific: Singapore, 2003; vol. 8.
(77) Lynch, B. J.; Fast, P. L.; Harris, M.; Truhlar, D. G. *J. Phys. Chem. A* **2000**, *104*, 4811−4815.
(78) Bürger, H.; Pawelke, G.; Rahner, A.; Appelman, E. H.; Halonen, L. *J. Mol. Spectrosc.* **1989**, *138*, 346−354.
(79) Duncan, J. L.; McKean, D. C.; Tullini, F.; Nivellini, G. D.; Perez Peña, J. *J. Mol. Spectrosc.* **1978**, *69*, 123−140.
(80) Shimanouchi, T. *Tables of molecular vibrational frequencies consolidated*; National Bureau of Standards: Gaithersburg, MD, 1972; Vol. I.
(81) Calculated structures and harmonic frequencies of all species, as well as the quartic force field of $CH_3CN \cdot HOF$, are available on the World Wide Web at http://theochem.weizmann.ac.il/web/papers/Rozen.html